

Integrated Radar and Missile System with Poisson-Prioritized Threat Management and PPN Guidance for Countering Multiple UAV Threats

Giselle Hage¹, Ari Santoso^{2*}, Mochammad Sahal³

^{1, 2, 3} Department of Electrical Engineering, Institut Teknologi Sepuluh Nopember, Surabaya, Indonesia
Email: ¹ 6022232027@student.its.ac.id, ² santoso@ee.its.ac.id, ³ sahal@its.ac.id

*Corresponding Author

Abstract—In military defense, critical infrastructure protection, and border and maritime surveillance, radar detection plays a critical role in neutralizing threats, since slight delays in detection can enable hostile UAVs to breach defenses and target critical objectives. This research proposes an air defense system, consists of integrated radar and missile system, to detect and neutralize aerial threats. The radar detects UAVs, tracks their trajectories, and prioritizes threats according to the distance of UAVs within its detection range, incorporating Poisson-distributed probability to dynamically allocate missile resources, allowing the systems to cover broader threat zones, which is crucial for the real-time interception of multiple UAVs. Each UAV is equipped with a state feedback controller for accurate navigation, while the missile system consistently enhancing its trajectory to accurately track and intercept threats under PPN guidance. Simulated experiments indicate that the proposed system intercepted the aerial threats within its operational range and time constraints in various battlefield scenarios. The system's effect within its operational radius has also been evaluated in an experiment designed to counter a swarm of 6 UAVs flies in a predefined formation. In this scenario, the air defense system successfully launched a missile towards UAV swarms that neutralized 83.33% of total identified threats. The proposed system can be an alternative air defense systems to confront UAV threats in battlefield situations, with potential application in disaster management, search and rescue, and early warning system.

Keywords—Integrated Radar and Missile System; Pure Proportional Navigation Guidance; UAV Defense System; UAV Swarm Neutralization.

I. INTRODUCTION

The increasing complexity of combat scenarios and operational constraints has reduced the effectiveness of individual Unmanned Aerial Vehicle (UAV) missions [1]–[5]. Multi-agent systems are used to enhance its efficiency in completing various tasks in the field of war environment, such as exploration, surveillance, search-and-rescue operations, and missions in complex war environments [6]–[14]. The development of aerial threats and their ability to evade detection has increased the demand for highly accurate radar systems capable of covering vast distances and rapidly identifying threats [15]–[17].

Radar's capability of early detection is crucial in detecting threats, since a slight delay allow threats to potentially causing damage to critical infrastructure or assets [18]–[25]. However, accurate detection is often difficult by the small

size and low radar cross-sections of UAVs, which can fit into environmental clutter [26]–[29]. To overcome these issues, radar systems have to be equipped with dynamic threats management strategies. By prioritizing threats based on real-time assessments, the system is capable of ensuring that the most dangerous threats are intercepted first [30]–[35].

Radar prioritizes threat detection using various indicators, such as a threat's proximity and severity, through frameworks like radar capability-based probability [36]–[40] and other probabilistic models that facilitate the efficient management of multiple threats simultaneously [41]–[46]. This approach ensures optimal utilization of radar resources by monitoring less critical targets while prioritizing more immediate threats [47]–[49]. However, as radar systems lack offensive capabilities, they rely on missile platforms for threat neutralization [50]–[53]. Thus, an effective air defense system should incorporate a radar for UAV detection, which, upon identifying a threat, activates and launches a missile targeting the detected position. Effective integration between radar and missile systems is crucial, as any communication gaps could result in delayed interceptions or missed targets [54]–[56].

Modeling potential collisions between missiles and UAVs based solely on probability may not fully reflect real-world dynamics, as missiles are designed to follow a predefined trajectory [57]–[64]. Extensive research on missile interception has explored various guidance laws, including proportional navigation (PN) and pure proportional navigation (PPN) [65]–[67]. PN-based algorithms adjust the missile's trajectory continuously based on the relative movement of the target, ensuring precise tracking even in high-speed scenarios [68]–[71]. PPN, specifically adapted for intercepting evasive UAVs, enables missiles to maintain a stable line of sight by dynamically reducing miss angles [72]–[74]. Integrated radar-missile communication platforms, which distribute real-time tracking data, have shown improved interception success rates in recent experiments, allowing for accurate engagement of multiple UAVs with minimal response times [75]–[78].

Although these defense systems provide critical protection, UAVs employ advanced tactics to evade interception [79]–[81]. Previous research applied controllers to each UAV to maintain flight stability and replicate UAV movement in the real world [82]–[85]. However, prior



researches in the field of air defense systems have not yet considered the realistic modeling of UAV movement, and often treating them as particles or using simple controllers that do not consider UAV dynamics. Their fast-moving behaviors complicate radar tracking, requiring continuous recalibration of threat assessments to account for real-time changes in UAV trajectories [86]–[87].

To address these challenges, defense systems require a comprehensive strategy that combines precise radar detection, efficient prioritization, and PPN-guided interception to address the complexities of multi-UAV operations [88]–[89]. This study proposes an air defense system that utilizes Poisson-distributed prioritization for optimized resource allocation while synchronizing radar and missile systems to improve interception performance. Simulations will evaluate the system's effectiveness against dynamic multi-UAV threats, offering valuable insights into how integrated radar and missile systems can sustain operational advantage in challenging scenarios.

This research proposed an integrated radar and missile system to detect, prioritize, and intercept threats. This approach uses a Poisson distributed prioritization to optimize missile resource allocation, and applies PPN guided missiles to ensure accurate interception towards fast moving targets. The proposed system is evaluated through several experiments which shows its effectiveness in various operational scenarios.

This study advances the field of defense systems by examining the interplay among radar, missiles, and UAVs in intricate environments, specifically:

- 1) This research demonstrates the capability of integrated radar and missile systems to effectively detect, prioritize, and neutralize multiple UAV threats, equipped with real-world controllers and dynamics.
- 2) Through simulation experiments, the study assesses how Poisson-based prioritisation, real-time resource allocation, and integrated missile under PPN guidance responses augment the performance of the defense system in scenarios characterised by multiple dynamic threats.

The paper is organized as follows. Section I examines the background of integrated radar and missile systems. Section II delineates the problem model, and formulates the detection and interception strategy. Section III presents the results and comments. Finally, section IV closes the work with conclusion and recommendations for future research.

II. METHOD

A. Problem Formulation

A fleet of N UAVs, denoted by UAV- i where $i \in \{1, 2, \dots, N\}$. Each UAV- i maintains a state vector $x_t^i = [x_t^i, y_t^i, z_t^i, \dot{x}_t^i, \dot{y}_t^i, \dot{z}_t^i, \phi_t^i, \theta_t^i, \psi_t^i, \dot{\phi}_t^i, \dot{\theta}_t^i, \dot{\psi}_t^i]$ representing its current position (x_t^i, y_t^i, z_t^i) , linear velocity $(\dot{x}_t^i, \dot{y}_t^i, \dot{z}_t^i)$, orientation $(\phi_t^i, \theta_t^i, \psi_t^i)$, and angular velocity $(\dot{\phi}_t^i, \dot{\theta}_t^i, \dot{\psi}_t^i)$ in the 3D space environment at time step t . Missiles are launched from radar stations upon detection of any UAV entering their detection range. Each missile follows a PPN-guided trajectory aimed at a detected UAV. To be noted, each

radar can only deploy one missile for the entire simulation. A missile's state is denoted by $\gamma_k(x) = [x_{M_k}(x), y_{M_k}(x), z_{M_k}(x)]$, representing its current position.

The problem formulation of this research is establishing an effective air defense mechanism and strategy in order to detect, track, and intercept an unauthorized threats which attempting to navigate through a defended environment. The radars are strategically positioned with specific detection ranges and altitudes, maximizing the likelihood of UAV detection. Radar designed to continuously monitors its operational area, and detects incoming threats in its operational range. When a UAV threat is detected, the radar initiates a response by launching an interceptor missile to the current position of the threats. The missile relies on line-of-sight data to refine its path, ensuring a successful interception.

The objective of the proposed system is to safeguarding airspace by preventing unauthorized threats in their operational zones, and ensuring the UAV threats is neutralized before it reaches its targets. To address this issue, the air defense system must excel in early detection, accurate tracking, and guided missile interception, so that the timely deployment of missiles toward the UAV can be achieved. This process demands optimized radar coverage and precision to ensure rapid interception.

The simulation in this study was conducted using MATLAB to calculate and visualize the results, including interception time, success rates, and tracking accuracy. Data was collected to evaluate the system's performance against UAV threats. Visualization was done through graphs and diagrams illustrating UAV flight paths and missile interceptions. The Quanser QDrone quadcopter was used as the UAV model, providing realistic flight dynamics for simulating interactions with the radar and missile systems in dynamic environments.

B. UAV Dynamics Model

The modeling of quadcopter is in the hybrid-frame, and the translational motion is derived from earth-fixed coordinates which define the quadcopter's relative position and velocity to the earth. Besides, rotational motion is modeled in the body fixed coordinates, B-frame, as rotational dynamics directly impact the quadcopter's movement. By applying Euler's first axiom and Newton's second law, the equation for translational motion is derived. The force F_i is the lifting force produced by each motor propeller which is defined as (1)–(2) as in [90]–[91],

$$F_i = K \frac{\omega}{s + \omega} u_i \quad (1)$$

$$\sum F^E = \ddot{\xi}^E m \quad (2)$$

$$F_f^E + F_g = \ddot{\xi}^E m \quad (3)$$

$$F_f^E = R_{\xi}^{BE} F_f^B \quad (4)$$

where the ω is cutoff frequency, s is Laplace variable, u_i is the input signal. ξ^E represents translational acceleration of the quadcopter in the E-frame, F_g represents gravitational force, F_f^E is aerodynamic drag force in the E-frame, and m is the mass of the quadcopter. The constant K is determined by flying the quadcopter in a hover state, which is proportional to the total lift force generated by the four quadcopter motors during hovering. R_{ξ}^{BE} represents rotation matrix to transform drag force F_f^B from the B-frame to E-frame.

Since the force acting is only along the z-axis, the resulting force is solely F_z , or the thrust force U_1 . The orientation angles is represented by roll (ϕ), pitch (θ), and yaw (ψ) angle.

$$F_f^E = \begin{bmatrix} U_1(\sin \psi \sin \phi + \cos \psi \sin \theta \cos \phi) \\ U_1(-\cos \psi \sin \phi + \sin \psi \sin \theta \cos \phi) \\ U_1(\cos \theta \cos \phi) \end{bmatrix} \quad (5)$$

Substituting (3) into (5) yields (6). This results in the quadcopter's translational motion equation as in (7)–(9),

$$F_f^E + \begin{bmatrix} 0 \\ 0 \\ -mg \end{bmatrix} = \begin{bmatrix} \ddot{X} \\ \ddot{Y} \\ \ddot{Z} \end{bmatrix} m \quad (6)$$

$$\ddot{X} = (\sin \phi \sin \psi + \cos \phi \sin \theta \cos \psi) \frac{U_1}{m} \quad (7)$$

$$\ddot{Y} = (-\sin \phi \cos \psi + \cos \phi \sin \theta \sin \psi) \frac{U_1}{m} \quad (8)$$

$$\ddot{Z} = -g + (\cos \phi \cos \theta) \frac{U_1}{m} \quad (9)$$

where $[\ddot{X}, \ddot{Y}, \ddot{Z}]$ represent the acceleration along the x , y , and z -axis of the E-frame consecutively.

Based on Euler's second axiom in Newton's second law, the rotational motion is described by (10), which is defined in E-frame coordinates, and must be transformed into B-frame coordinates, resulting to (12). If the derivative of the transformation matrix T_{θ} is $T_{\theta}S(\omega^B)$, where $S(\omega^B)$ is a skew-symmetric matrix, then (11) can be rewritten as (12).

$$\tau^E = J\ddot{\Theta}^E \quad (10)$$

$$T_{\theta}\tau^B = J(T_{\theta}\omega^B + T_{\theta}\dot{\omega}^B) \quad (11)$$

$$T_{\theta}\tau^B = T_{\theta}(\omega^B \times J\omega^B + J\dot{\omega}^B) \quad (12)$$

$$J\dot{\omega}^B = -(\omega^B \times J\omega^B) + \tau^B \quad (13)$$

Solving (13) results in (14).

$$\begin{bmatrix} J_{xx}\dot{p} \\ J_{yy}\dot{q} \\ J_{zz}\dot{r} \end{bmatrix} = \begin{bmatrix} (J_{yy} - J_{zz})qr \\ (J_{zz} - J_{xx})pr \\ (J_{xx} - J_{yy})pq \end{bmatrix} + \begin{bmatrix} U_2l \\ U_3l \\ U_4d \end{bmatrix} \quad (14)$$

Thus, the translational motion equation is obtained as in (15)–(17).

$$\dot{p} = \frac{J_{yy} - J_{zz}}{J_{xx}}qr + \frac{U_2l}{J_{xx}} \quad (15)$$

$$\dot{q} = \frac{J_{zz} - J_{xx}}{J_{yy}}pr + \frac{U_3l}{J_{yy}} \quad (16)$$

$$\dot{r} = \frac{J_{xx} - J_{yy}}{J_{zz}}pq + \frac{U_4d}{J_{zz}} \quad (17)$$

The quadcopter dynamics model used in this paper defined by (7)–(9) and (15)–(17). The parameters used defined in Table I.

TABLE I. PARAMETERS OF QUADCOPTER DYNAMICS

Parameter	Values
m	1 kg
g	9.81 m/s ²
J_{xx}	0.03 kg.m ²
J_{yy}	0.03 kg.m ²
J_{zz}	0.04 kg.m ²
l	0.2 m
d	3.13×10^{-5} N

C. State Feedback Controller

The quadcopter control scheme used as a controller is divided into position control as an outer loop and attitude control as an inner loop which can be seen in Fig. 1 [90]–[91]. In position control, the input is the error value of the reference position to the actual quadcopter position $[X(t) Y(t) Z(t)]$. The output of position control is U_1 , $s_{7ref}(t)$, and $s_{8ref}(t)$. The quadcopter angular position $[\phi(t) \theta(t) \psi(t)]$ become input for attitude control which produces outputs U_2 , U_3 , and U_4 that consecutively imply roll, pitch, and yaw forces.

The state feedback controller is used to control the altitude (Z) and heading (ψ). The combination of state feedback controller and proportional-derivative (PD) controller is used to control the positions X and Y and attitudes ϕ and θ . This control scheme is used for all quadcopters, since it is assumed that all quadcopters used in this research are identical and homogenous. Overall, the PD state feedback controller is used to control the movement of the quadcopter starting from the point where the UAV starts moving towards the target point according to the trajectory that has been generated.

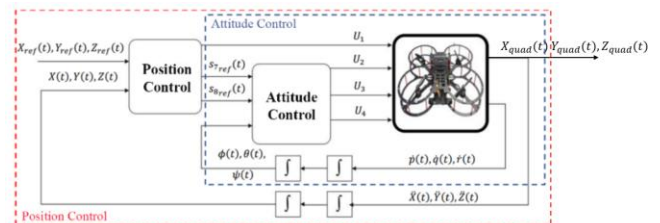


Fig. 1. Block diagram of quadcopter's attitude and position control using state feedback controller [90] (ganti ujung output)

To control altitude using a state feedback controller, (9) must be modified by including air drag forces, resulting in the following state equation,

$$\ddot{z} = -g + \frac{(\cos \phi \cos \theta)U_1}{m} - d\dot{z} \quad (18)$$

where

$$U_1 = g + K_1(z_{ref} - z) + L_1(\dot{z}_{ref} - \dot{z}) + \ddot{z}_{ref} + d\dot{z} \quad (19)$$

by substituting (19) to (18), (20) is obtained.

$$U_1 = g + K_1(z_{ref} - z) + L_1(\dot{z}_{ref} - \dot{z}) + \ddot{z}_{ref} + d\dot{z} \quad (20)$$

The heading of the quadcopter will be controlled with a state feedback controller as a regulator to ensure that $\psi \rightarrow 0$.

$$U_4 = \frac{J_{zz}}{d} (-K_4\psi - L_4\dot{\psi}) \quad (21)$$

$$\dot{r} = \frac{J_{xx} - J_{yy}}{J_{zz}} pq - K_4\psi - L_4\dot{\psi} \quad (22)$$

$$\dot{r} = -K_4\psi - L_4\dot{\psi} \quad (23)$$

When the quadcopter reaches the desired position or target, the target acquisition control will become active. A proportional-derivative controller is used to manage the X and Y positions to generate outputs that will serve as reference inputs for the attitude control of ϕ and θ . Since the heading (ψ) is controlled by the state feedback controller as a regulator ($\psi \rightarrow 0$), (7) can be simplified to (24).

$$\ddot{X} = \cos \phi \sin \theta \frac{U_1}{m} \quad (24)$$

$$U_2 = \frac{J_{xx}}{I} (K_2 s_{7ref} - K_2 s_7 - L_2 \dot{s}_{7ref} - L_2 \dot{s}_7 + \ddot{s}_{7ref}) \quad (25)$$

$$\ddot{Y} = -\sin \phi \frac{U_1}{m} \quad (26)$$

$$U_3 = \frac{J_{yy}}{I} (K_3 s_{8ref} - K_3 s_8 - L_3 \dot{s}_{8ref} - L_3 \dot{s}_8 + \ddot{s}_{8ref}) \quad (27)$$

The parameters used in (24)–(27) are listed in the Table II.

TABLE II. PARAMETERS OF PROPORTIONAL- DERIVATIVE STATE FEEDBACK CONTROLLER

Parameter	Values
K_1	16
K_2	100
K_3	100
K_4	0.09
L_1	9
L_2	21
L_3	21
L_4	0.61

D. Integrated Radar and Missile Model

A radar can find a UAV in its mission space with a certain probability. Factors that affect the probability of radar detection generally include the curvature of the earth, atmospheric refraction and absorption, ground clutter interference, the distance between the UAV and the radar, and so on. The radar utilizes electromagnetic waves which propagate in a linear trajectory. The energy loss from the radar's produced energy wave, upon reflection by a target, is inversely proportional to the fourth power of the one-way propagation distance of the electromagnetic wave (R^4) [93]. It is assumed that the probability distribution of the radar finding a target uses a Poisson distribution. Assuming the maximum range of the radar at a height h is R_h , the target detection probability can be estimated as the following equation.

$$P_R = \begin{cases} \frac{R^4}{R_h^4 + R^4}, & R \leq R_h \\ 0, & R > R_h \end{cases} \quad (28)$$

Assuming that the radar is able to identify the UAV, the missile will be fired in the direction of the current location of the UAV, as shown in Fig. 2. The process begins with target detection, followed by threat prioritization using Poisson-based probability and threat evaluation to assess the severity of the identified targets. Once the UAV is confirmed, the missile is launched toward its estimated position based on radar data. The missile, presumed to be a passive seeker, is guided under Proportional Navigation (PPN) with an initial Line of Sight (LoS) angle defined by azimuth (α_M) and elevation (ϵ_M) to intercept the target accurately [94].

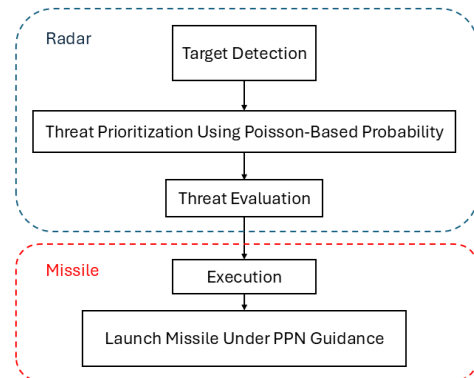


Fig. 2. Algorithm of 3-D simulation of the movement of missile under PPN guidance launched from radar position towards single UAV's target position

In order to intercept UAV threats in real time, the Algorithm 1 delineates the process of incorporating radar detection with missile deployment. Radar stations incessantly monitor UAVs, determining the distance from each UAV to the radar station to evaluate if the UAV falls within a specified detection range. The critical metric, R_h , dynamically modifies the detection threshold in accordance with the UAV's height. Upon a UAV entering the radar's detection range, the system calculates a detection probability, P_R , to assess the priority for missile deployment. If the probability rises beyond a predetermined threshold, the missile will be launched.

Algorithm 1 Radar System

```

1: Initialize environment with N UAVs and M targets
2: Initialize radar stations and missile systems
3: Initialize UAV positions and set their goals
4: for each time step  $t = 1$  to  $T$  do:
5:   for each radar station  $r$  do:
6:     for each UAV  $j$  do:
7:       Compute distance between UAV and radar:
        $d_r(\mathbf{u}_i) = \sqrt{(x_i - x_r)^2 + (y_i - y_r)^2}$ 
8:       Compute  $R_h$ :
        $R_h = R_{max} - \frac{R_{max} + R_{min}}{2} |z_i - \frac{h_{max}}{2}|$ 
9:       if  $d_r \leq R_h$ :
10:        Compute  $P_R(\mathbf{u}_i) = \frac{d_r(\mathbf{u}_i)^4}{R_h^4 + d_r(\mathbf{u}_i)^4}$ 
11:        if  $PR > \max\_prob$ :
12:          launch missile as Algorithm 1
13:        end if
14:      end if
15:    end for
16:  end for
17: end for

```

PPN maintains a proportional relationship between the rate of closure and lateral acceleration. Missile continuously adjusts its acceleration perpendicular to its velocity vector to ensure alignment with the target by reacting to the angular rate of the LoS between the missile and the target. This guidance method minimizes the need for detailed information about the target's speed or trajectory, relying instead on angle-only measurements from passive sensors, such as azimuth and elevation rates, thereby reducing computational demands. PPN guidance typically separates missile flight into a high-acceleration boost phase and a sustained lower-acceleration phase. In these phases, a fixed navigation constant controls the proportional adjustment rate in response to shifts in Line of Sight (LoS) angles. By prioritizing angle-based corrections, the PPN model facilitates efficient, real-time targeting adjustments, which are vital for dynamic interception scenarios. This makes PPN an effective strategy in scenarios requiring rapid response and minimal computational complexity, such as missile defense and close-range threat engagement systems. The equation for missile's PPN guidance law are as in [94].

Upon launch, the missile possesses an initial velocity v_{M_0} and a boost acceleration a_{M_b} aligned with the missile's velocity vector. Subsequent to a designated duration ξ_b , the missile transitions into the sustain phase characterized by a reduced acceleration a_{M_s} . The acceleration vector is orthogonal to the missile's velocity vector. The horizontal and vertical components of missile acceleration, a_{M_α} and a_{M_ε} , are orthogonal to both the missile velocity and the line of sight angular velocity, their magnitudes defined as in (29)–(30),

$$a_{M_\alpha} = cv_{M_k} \dot{\alpha}_{M_k} \quad (29)$$

$$a_{M_\varepsilon} = cv_{M_k} \dot{\varepsilon}_{M_k} \quad (30)$$

where c is the navigation constant, $\dot{\alpha}_{M_k}$ and $\dot{\varepsilon}_{M_k}$ are the LoS azimuth and elevation velocities of the missile towards the target, and k denotes discrete time.

Given (29)–(30), the magnitudes of the angular rates of rotation from the velocity of the missile, $|\omega_{\alpha_k}|$ and $|\omega_{\varepsilon_k}|$, defined as (31)–(32).

$$|\omega_{\alpha_k}| = \left| \frac{a_{M_\alpha k}}{v_{M_k}} \right| = |c \dot{\alpha}_{M_k}| \quad (31)$$

$$|\omega_{\varepsilon_k}| = \left| \frac{a_{M_\varepsilon k}}{v_{M_k}} \right| = |c \dot{\varepsilon}_{M_k}| \quad (32)$$

In order to enhance the realism of the model used in this research, the maximum turning speed of the azimuth angle Ω_α and elevation angle Ω_ε is used in the evolution of the LoS angle, so that the updated azimuth and elevation equation defined in (33)–(34),

$$\alpha_{M_{k+1}} = \begin{cases} \alpha_{M_k} + c \dot{\alpha}_{M_k} T, & |\omega_{\alpha_k}| \leq \Omega_\alpha \\ \alpha_{M_k} + \text{sign}[c \dot{\alpha}_{M_k}] \Omega_\alpha T, & \text{otherwise} \end{cases} \quad (33)$$

$$\varepsilon_{M_{k+1}} = \begin{cases} \varepsilon_{M_k} + c \dot{\varepsilon}_{M_k} T, & |\omega_{\varepsilon_k}| \leq \Omega_\varepsilon \\ \varepsilon_{M_k} + \text{sign}[c \dot{\varepsilon}_{M_k}] \Omega_\varepsilon T, & \text{otherwise} \end{cases} \quad (34)$$

where T represents the sample interval, ω_{α_k} and ω_{ε_k} consecutively represent angular velocity of azimuth and elevation LoS.

In the other hand, the missile velocity defined as (35),

$$v_{M_{k+1}} = v_{M_k} + a_{M_{||k}} T \quad (35)$$

$$a_{M_{||}} = \frac{T_p - D_p}{M_p} \quad (36)$$

where $a_{M_{||}}$ denoting the acceleration component of the missile velocity vector. In the boost phase, $a_{M_{||}}$ is replaced by a_{M_b} and a_{M_s} in the sustain phase. T_p , D_p , and M_p denote the thrust, drag, and mass of the missile, respectively. For estimation purposes, a constant net-specific thrust is presumed, as drag escalates with velocity and mass diminishes during each phase. Consequently, a_{M_b} and a_{M_s} are presumed to be constant during each phase.

The discrete time state equation of the missile movement is shown by (37)–(39) [94].

$$x_{M_{k+1}} = x_{M_k} + v_{M_k} \cos \varepsilon_{M_k} \cos \alpha_{M_k} T \quad (37)$$

$$y_{M_{k+1}} = y_{M_k} + v_{M_k} \cos \varepsilon_{M_k} \sin \alpha_{M_k} T \quad (38)$$

$$z_{M_{k+1}} = z_{M_k} + v_{M_k} \sin \varepsilon_{M_k} T \quad (39)$$

The missile trajectory is then obtained through the PPN guidance law. The vector $\gamma_k(x)$ is a vector consisting of the missile position components at time k .

$$\gamma_k(x) = [x_{M_k}(x) \quad y_{M_k}(x) \quad z_{M_k}(x)]' \quad (40)$$

Algorithm 2 below outlines the state update of the missile.

Algorithm 2 Missile System

- 1: Initialize missile_state, parameters, azimuth and elevation angle
 - 2: **for** each time step $t = 1$ to T **do**:
 - 3: Compute euclidean distance rel_dist to target
 - 4: **if** $rel_dist < 2$ meters:
 - 5: set intercepted = true
 - 6: **end if**
 - 7: Compute missile acceleration as (29)–(30)
 - 8: Update LoS angular rates as (31)–(32)
 - 9: Update missile LoS angles as (33)–(34)
 - 10: **if** elapsed_time \leq boost_time:
 - 11: $a_parallel = (Tp_boost - Dp) / Mp$
 - 12: **else**:
 - 13: $a_parallel = (Tp_sustain - Dp) / Mp$
 - 14: **end if**
 - 15: Compute velocity and acceleration as (35)–(36)
 - 16: Update missile position as (37)–(39)
 - 17: **end for**
-

III. RESULTS AND DISCUSSION

A. Setup

In this research, the missile system employs pure proportional navigation (PPN) guidance, which allows the missile to adjust its trajectory dynamically to intercept the target accurately. Meanwhile, the UAV utilizes a state feedback controller to navigate, simulating the behavior and response patterns of real-world UAVs. Throughout the missile's flight, the missile system continuously updates the UAV's position towards its LoS angle, refining the missile's trajectory in real time to counter UAV evasive maneuvers. If another UAV enters the radar's detection zone with a higher threat level, the system reallocates resources accordingly, ensuring that the most immediate threat is prioritized.

These experiments adopt several limitations to make the simulation as close to realistic applications as possible, which in turn brings out the relevance and practicality of the study better. One of the basic conditions is that if the minimum distance between a UAV and a missile is less than 2 meters, the missile is already considered to have intercepted the UAV successfully. From its launch, the missile system must intercept the UAV within 5 seconds. If this time limit is surpassed, the missile will be intercepted at its current position, regardless of whether it has reached the UAV or not.

The interaction among radar, missiles, and UAVs evolves dynamically at each time step, with the system continuously recalculating detection probabilities and interception paths based on UAV behavior. This study involves three experiments, each aimed at simulating different levels of complexity in the environment and the target. The real-time interaction between radar and missile systems highlights the critical role of air defense strategies in managing multiple, high-risk UAV threats simultaneously.

B. Experiments on Single UAV

This experiment demonstrates a missile interception scenario where a UAV is detected and neutralized within a predefined radar detection zone. The radar cone serves as the detection boundary, ensuring that the UAV's movement can be continuously monitored. It is assumed that UAV do not know the detection range of the radar. As the UAV moves along its trajectory, the missile is guided towards it based on real-time tracking data. The plotted trajectories for both the UAV and the missile confirm the system's ability to maintain precise paths, converging at the interception point.

The first experiment involved a single UAV and a radar that is assumed can deploy only one missile for the whole simulation. As in Fig. 3, the final interception occurred at [829.179, 829.502, 99.3031] with a minimum separation between missile and UAV of 1.5662 meters. The distance between UAV threat and missile showed in Fig. 4. This minimal distance at the point of interception is within the minimum threshold 2 meter, suggests the missile's guidance mechanism successfully intercept the threat in this experiments.

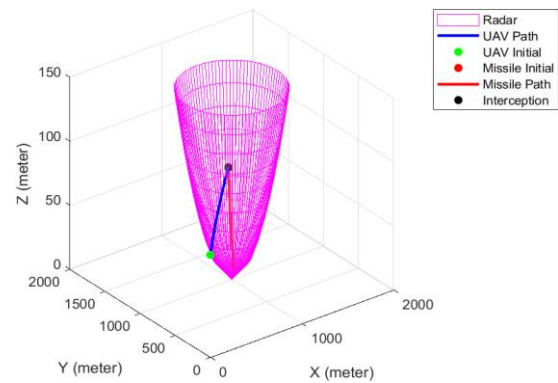


Fig. 3. The 3-D simulation of the movement of missile under PPN guidance launched from radar position towards single UAV's target position

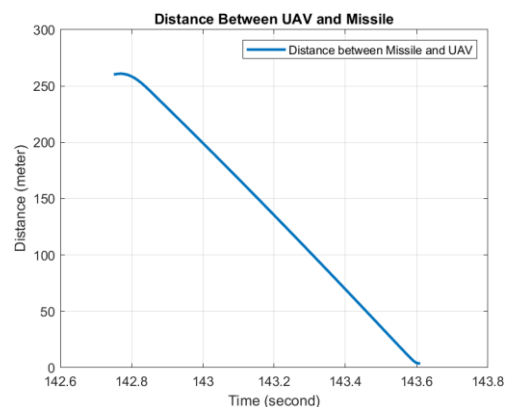


Fig. 4. Distance between UAV and missile from simulation on Fig. 2. The x-axes imply the iterations while the y-axes imply the distance

As in Fig. 5, we experiments the system's capability if there are two UAVs entering the same radar sequentially. The green points show the initial position of each UAV, and the red points show the goal position of each UAV. The center of the radar defined at [1000, 1000, 0], within the maximum radius 500 meters. It is shown that the first UAV entering the radar will be the target of missile interception, while another UAV still reach their goal.

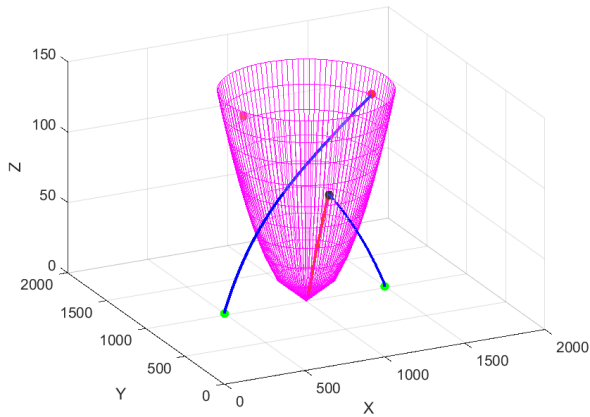


Fig. 5. The simulation of 2 UAVs entering a radar sequentially. Missile launched towards the first UAV entering radar. All axes is represented in meter

However, if there are two UAVs entering the same radar in the same time, a missile will be launched towards the UAV with highest probability defined in (28). As in Fig. 6 and Fig. 7, radar checking those two UAVs in the same time with detection probability 0.1201 and 0.3598, consecutively for UAV 1 and 2. Therefore, missile intercepted UAV 2 at position [1198.78, 1000, 49.82], with minimum distance between missile and UAV is 1.23 meters, showed in Fig. 8. The minimal distance at the point of interception is within the minimum treshold 1 meter, shows that missile successfully intercepted the UAV threat, especially the one with highest Poisson-distributed probability.

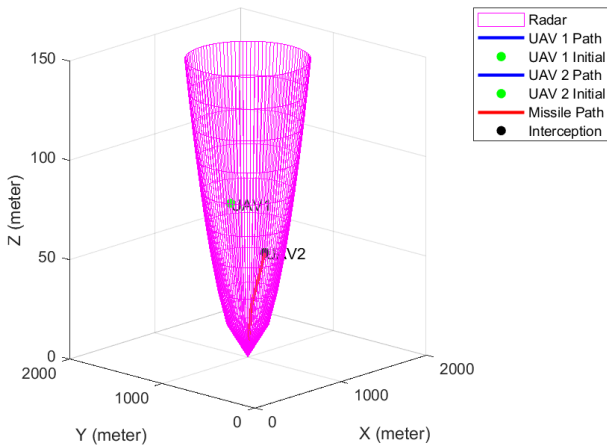


Fig. 6. The simulation of 2 UAVs entering a radar. Missile launched towards UAV with higher probability based on (38)

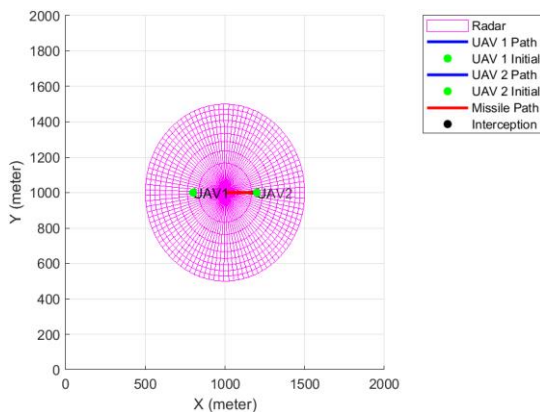


Fig. 7. Look up point of view of Fig. 6

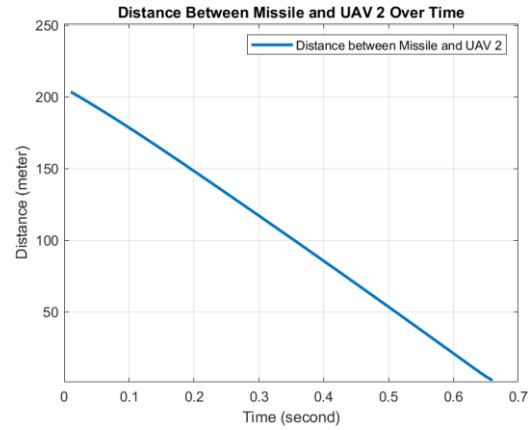


Fig. 8. Distance between UAV and missile from simulation on Fig. 5

C. Experiments on Multiple Radars and UAVs

In this simulation, the defense system is operated within a circumscribed 3D environment, with limits established at [0, 5000] meters along the x and y axes and a height of 100 meters. The threats' initial position are defined in Table III and Table IV. Four radar stations are strategically located to oversee airspace for UAV activities. These stations perpetually monitor for UAVs entering their detection zones, calculating distances between each UAV and the radar to ascertain whether the UAV is within range. The detection threshold, denoted as R_h , adapts dynamically according to the UAV's altitude in relation to the radar's height restriction, accounting for both horizontal and vertical constraints. Each radar has a predefined maximum range 800 m and minimum range 200 m, along with a height limit 100 m. The environment showed in Fig. 9.

TABLE III. MULTI-UAVS INITIAL POSITION

UAV-	Position [x, y, z]
1	[0, 1720.63, 42.62]
2	[0, 3524.44, 81.8]
3	[0, 3673.34, 19.8]
4	[0, 3636.47, 26.18]
5	[3113.6, 0, 73.43]
6	[2535.55, 0, 84.19]
7	[4068.63, 0, 19.4]

TABLE IV. RADAR POSITION

Radar-	Position [x, y, z]
1	[1500, 3750, 0]
2	[1000, 1250, 0]
3	[3000, 1250, 0]
4	[3500, 3650, 0]

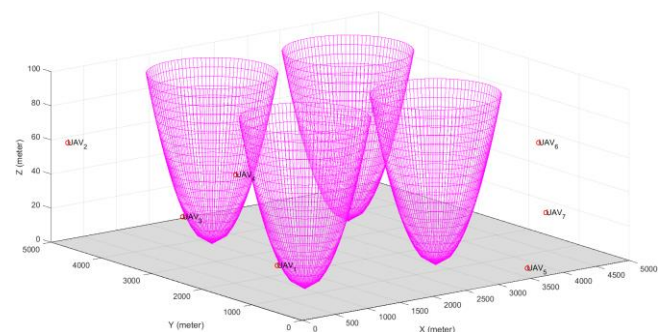


Fig. 9. The 3-D simulation environment on multi-UAVs

In Fig. 10 and Fig. 11, it is shown that radar 2 detects UAV 1, and radar 4 detects UAV 3. Each of them successfully launches a missile towards UAV's current position. The interception occurred at position [639.69, 1065.61, 45.88] and [3070.04, 3827.07, 49.87]. The detailed plot of distance between missile and their respective targets over time can be seen in Fig. 12. The continuous distance tracking shows the precision of missile guidance systems and their ability to maintain a decreasing trajectory towards the target until interception.

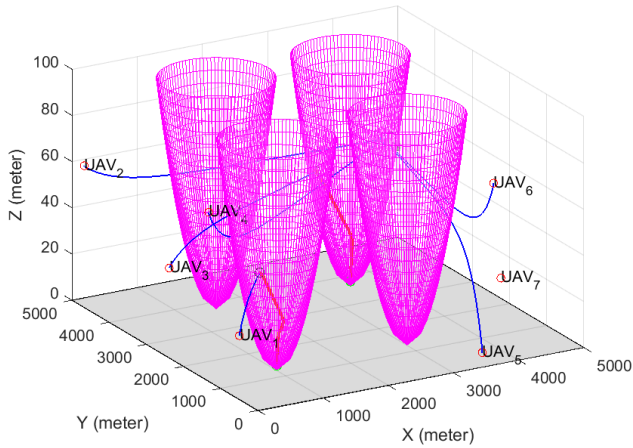


Fig. 10. The 3-D simulation environment, including multi-UAVs, multi-target, and the radar visualization

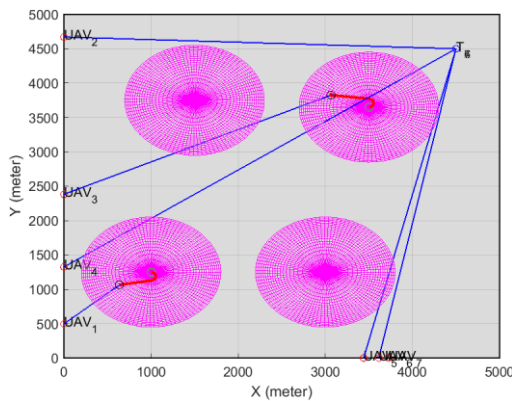


Fig. 11. The 3-D simulation environment, including multi-UAVs, multi-target, and the radar visualization

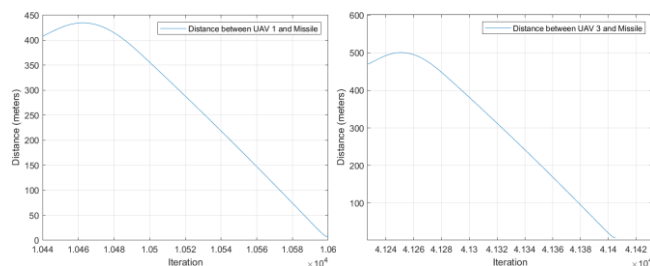


Fig. 12. Distance between UAV 1 and 3 towards missile

To be noted, the radar cone expands from a smaller radius at the base to a larger radius as it extends upwards. In Fig. 11, some UAVs appear to be moving inside the radar cone but are not intercepted by the missile. Upon closer inspection, UAV 3 does not move inside radar 3, UAV 4 does not move inside radar 2, and UAV 5 does not move inside radar 3. To provide clarity, Fig. 13 to Fig. 15 offers a different perspective that validates our earlier statement.

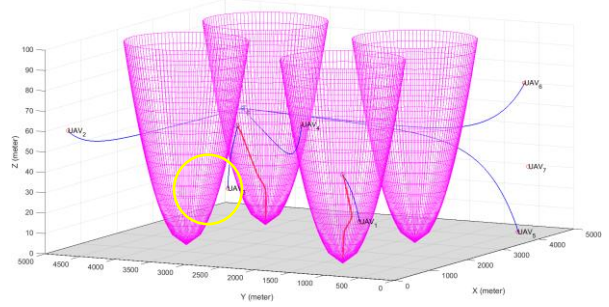


Fig. 13. Closer inspection of experiment in Fig. 9 that shows UAV 3 does not move inside radar 3

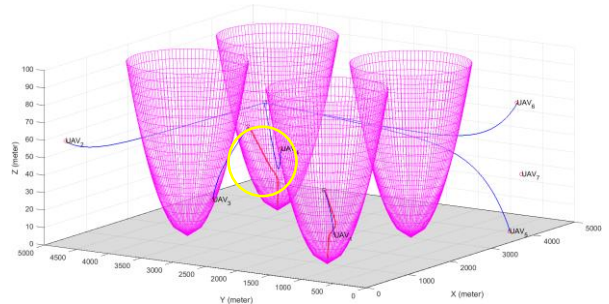


Fig. 14. Closer inspection of experiment in Fig. 9 that shows UAV 4 does not move inside radar 2

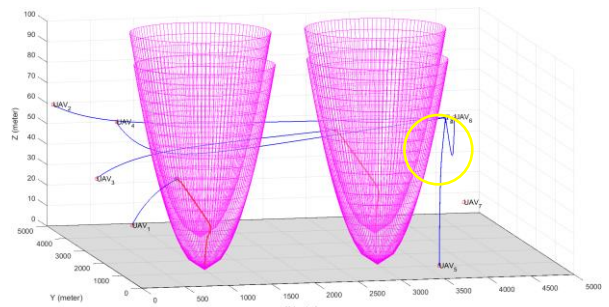


Fig. 15. Closer inspection of experiment in Fig. 9 that shows UAV 5 does not move inside radar 3

D. Experiments on UAV Swarm

In this experiment, a formation of UAVs maneuvers strategically towards a common aim. The environment features a radar system designed to identify possible UAV threats, consistently monitoring their movement. This radar is considered to possess more capabilities relative to earlier experimental configurations, as it can launch a missile with precise targeting, capable of neutralizing threats within a 5-meter radius from the interception point. The main objective of this experiment is to assess the possible damage caused by the missile within its operational range. Evaluating this damage radius is crucial, as practical applications prefer missiles capable of incapacitating many UAVs concurrently, so that the defense system can operate efficiently.

The initial position of each UAV illustrated in Fig. 16, and detailed in Table V. The UAV swarm moves along towards their common goal at [1800, 1800, 75]. The environment equipped with radar at [2500, 2500, 0] with maximum range 2000 meters and maximum altitude 150 meters. As in Fig. 17 and Fig. 18, the radar successfully detected and engaged UAVs within its operational range. It is shown that the missile intercepted UAVs at [1523.95,

1520.65, 75.74] at 262.02 seconds. This interception highlights the accuracy and responsiveness of the proposed air defense system, effectively neutralizing the detected threats with minimal deviation from the intended interception point.

TABLE V. MULTI-UAVS INITIAL POSITION

UAV-	Position [x, y, z]
1	[0, 0, 75]
2	[3, 0, 75]
3	[6, 0, 75]
4	[1.5, 2.598, 75]
5	[4.5, 2.598, 75]
6	[3, 5.196, 75]

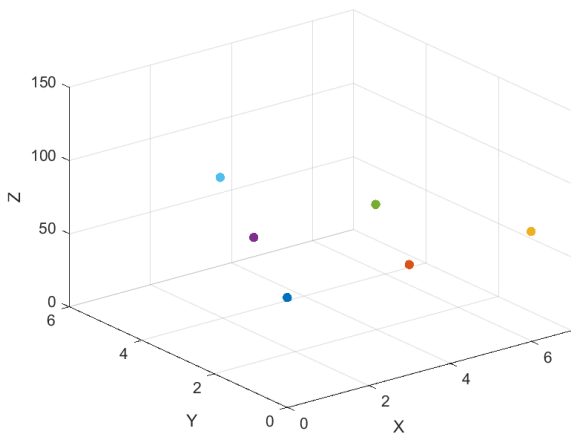


Fig. 16. Initial position for multi-UAVs threats in triangle shape formation consists of 6 UAVs. All axes represented in meters

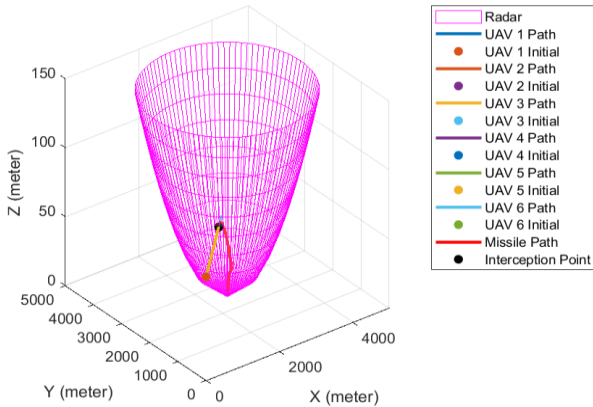


Fig. 17. The experiments on UAV swarm. The UAV swarm moves from its initial formation towards their common goal

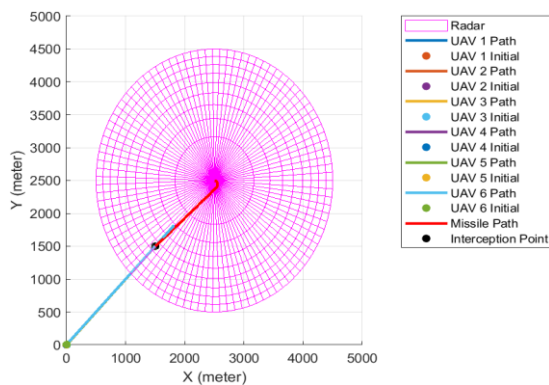


Fig. 18. The look up view for the experiment on UAV swarm

Missile successfully intercepted five out of six UAVs. Throughout the experiment, only UAV 6 survived the missile interception, since its distance from the missile was 5.46 meters, exceeding the threshold of 5 meters. The detailed distance between missile and UAV swarm at interception point listed in Table VI and Fig. 19 and Fig. 20. This experiment shows that within its specified radius, the designed air defense system is able to accurately neutralize grouped targets while within range.

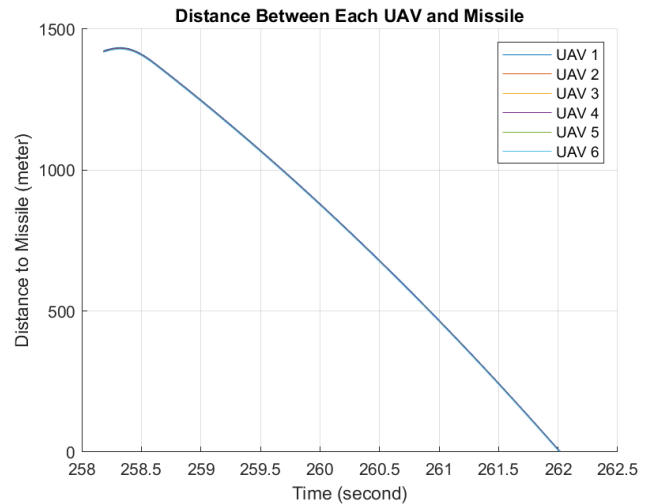


Fig. 19. The distance between missile and UAVs in experiments on UAV swarm

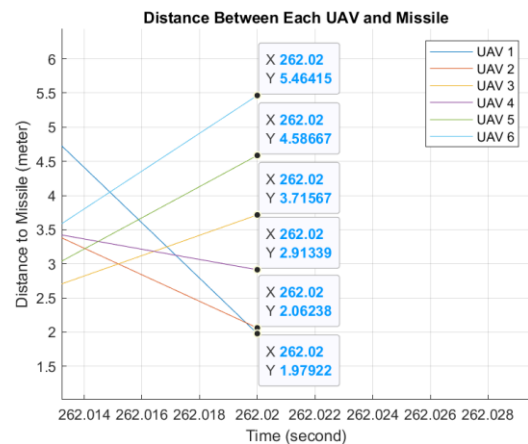


Fig. 20. The distance between missile and UAVs in experiments on UAV swarm at interception point

TABLE VI. DISTANCE BETWEEN UAVS AND MISSILE AT INTERCEPTION POINT

UAV-	Minimum Distance
1	5.46415
2	4.58667
3	3.71567
4	2.91339
5	2.06238
6	1.97922

Missile successfully intercepted five out of six UAVs. Throughout the experiment, only UAV 6 survived the missile interception, since its distance from the missile was 5.46 meters, exceeding the threshold of 5 meters. The detailed distance between missile and UAV swarm at interception point listed in Table VI and Fig. 19 and Fig. 20. This

experiment shows that within its specified radius, the designed air defense system is able to accurately neutralize grouped targets while within range.

Table VII provides a detailed comparison of the overall experimental configurations used to evaluate the performance of the proposed UAV detection and interception system. In the simplest configuration, involving one radar and one UAV, the system successfully detected and intercepted the UAV with a minimum distance of 1.5662 meters and an interception time of 0.9 seconds. For the configuration with one radar and two UAVs, the system detected two UAVs and successfully intercepted one, achieving a minimum interception distance of 1.23 meters with a reduced interception time of 0.65 seconds.

In a more complex configuration involving four radars and seven UAVs, the system detected and intercepted two UAVs. The minimum interception distances ranged between 1.87 and 1.37 meters, with interception times varying from 1.6 to 2.3 seconds. Finally, in the configuration involving one radar and six UAVs, the system demonstrated its scalability by detecting all six UAVs and successfully intercepting five. The minimum interception distances in this scenario varied from 1.98 meters to 5.46 meters, with an overall interception time of 3.72 seconds.

These results show the system's capability to handle increasingly complex scenarios, demonstrating reliable functionality in both single-UAV and multi-UAV environments. The variation in minimum distances and interception times across configurations highlights the system's effectiveness in addressing dynamic UAV threats.

TABLE VII. COMPARISON BETWEEN OVERALL EXPERIMENTS

Experiment Configuration	Detected UAV	Intercepted UAV	Minimum Distance (m)	Interception Time (s)
1 Radar and 1 UAV	1	1	1.5662	0.9
1 Radar and 2 UAVs	2	1	1.23	0.65
4 Radar and 7 UAVs	2	2	[1.87, 1.37]	[1.6, 2.3]
1 Radar and 6 UAVs	6	5	[1.98, 2.06, 2.91, 3.72, 4.59, 5.46]	3.72

IV. CONCLUSION

The proposed air defense system, integrating radar and missile components, effectively countered UAV threats across various scenarios. In the 1 radar and 1 UAV setup, the system intercepted the UAV within 1.5662 meters in 0.9 seconds. For 1 radar and 2 UAVs, it intercepted one UAV at 1.23 meters in 0.65 seconds. In the 4 radar and 7 UAVs scenario, it intercepted two UAVs with distances of 1.87 and 1.37 meters in 1.6 to 2.3 seconds. For 1 radar and 6 UAVs, five UAVs were intercepted with distances ranging from 1.98 to 5.46 meters in 3.72 seconds. These results confirm the system's capability to detect, track, and neutralize UAV threats in both simple and complex environments.

The future work could focus on enhancing capability of the system to more complex scenarios involving the heterogenous targets, higher numbers of UAVs, and complex dynamic threats incorporating advanced machine learning algorithms. The real-world implementation also can be considered, such as weather conditions, radar jamming, or signal interference. Enhancing the system's performance by incorporating energy efficiency and time-critical decision-making strategies could further strengthen its application in real-world air defense systems. The system also can be used for broader implications, such as disaster management.

ACKNOWLEDGMENT

This research was funded by Institut Teknologi Sepuluh Nopember, Surabaya, Indonesia.

REFERENCES

- [1] J. Li *et al.*, "RTPN method for cooperative interception of maneuvering target by gun-launched UAV," *Mathematical Biosciences and Engineering: MBE*, vol. 19, no. 5, pp. 5190-5206, 2022.
- [2] M. Moreira, E. Papp, and R. Ventura, "Interception of Non-Cooperative UAVs," *2019 IEEE International Symposium on Safety, Security, and Rescue Robotics (SSRR)*, pp. 120-125, 2019, doi: 10.1109/SSRR.2019.8848952.
- [3] A. Yang, X. Liang, Y. Hou, and M. Lv, "An Autonomous Cooperative Interception Method With Angle Constraints Using a Swarm of UAVs," *IEEE Transactions on Vehicular Technology*, vol. 72, pp. 15436-15449, 2023, doi: 10.1109/TVT.2023.3298635.
- [4] N. Jia, Z. Yang, and K. Yang, "Operational Effectiveness Evaluation of the Swarming UAVs Combat System Based on a System Dynamics Model," *IEEE Access*, vol. 7, pp. 25209-25224, 2019, doi: 10.1109/ACCESS.2019.2898728.
- [5] Q. Yang, J. Zhang, G. Shi, J. Hu, and Y. Wu, "Maneuver Decision of UAV in Short-Range Air Combat Based on Deep Reinforcement Learning," *IEEE Access*, vol. 8, pp. 363-378, 2020, doi: 10.1109/ACCESS.2019.2961426.
- [6] N. Gomez, N. Pena, S. Rincon, S. Amaya, and J. Calderon, "Leader-follower Behavior in Multi-agent Systems for Search and Rescue Based on PSO Approach," *Conference Proceedings - IEEE SOUTHEASTCON*, vol. 2022-March, pp. 413-420, 2022, doi: 10.1109/SoutheastCon48659.2022.9764133.
- [7] J. Hu, H. Niu, J. Carrasco, B. Lennox, and F. Arvin, "Voronoi-Based Multi-Robot Autonomous Exploration in Unknown Environments via Deep Reinforcement Learning," *IEEE Trans. Veh. Technol.*, vol. 69, no. 12, pp. 14413-14423, 2020, doi: 10.1109/TVT.2020.3034800.
- [8] N. Patrinoopoulou, I. Daramouskas, D. Meimetis, V. Lappas, and V. Kostopoulos, "A Multi-Agent System Using Decentralized Decision-Making Techniques for Area Surveillance and Intruder Monitoring," *Drones*, vol. 6, no. 11, 2022, doi: 10.3390/drones6110357.
- [9] B. G. Elkilany, A. A. Abouelsoud, A. M. R. Fathelbab, and H. Ishii, "A proposed decentralized formation control algorithm for robot swarm based on an optimized potential field method," *Neural Comput. Appl.*, vol. 33, no. 1, pp. 487-499, 2021, doi: 10.1007/s00521-020-05032-0.
- [10] M. Sahal, T. Agustinah, A. Jazidie, and H. Du, "Strategic Control in Cooperative Multi-Agent Moving Source Seeking with Obstacles Avoidance," *Int. J. Intell. Eng. Syst.*, vol. 16, no. 5, 2023.
- [11] X. Cao, M. Li, Y. Tao, and P. Lu, "HMA-SAR: Multi-Agent Search and Rescue for Unknown Located Dynamic Targets in Completely Unknown Environments," in *IEEE Robotics and Automation Letters*, vol. 9, no. 6, pp. 5567-5574, June 2024, doi: 10.1109/LRA.2024.3396097.
- [12] V. C. Maynad, Y. E. Nugraha, A. Alkaff, and C. Author, "Three-Dimensional Coordination Control of Multi-UAV for Partially Observable Multi-Target Tracking," *J. Res. Comput.*, vol. 5, no. 5, pp. 1227-1240, 2024, doi: 10.18196/jrc.v5i5.22560.
- [13] M. Sahal, T. Agustinah, and A. Jazidie, "Distributed Velocity Control in Cooperative Multi-Agent Moving Source Seeking," *Przegląd Elektrotechniczny*, vol. 2023, no. 8, 2023.

- [14] V. M. Nuzhdin, A. E. Ananenko, and D. V. Marin, "Radar of complex UAV detection and neutralization," in *Proc. 2021 Syst. Signals Generating Process. Field On-Board Commun.*, pp. 1–4, 2021.
- [15] M. N. Alpdemir, "Tactical UAV path optimization under radar threat using deep reinforcement learning," *Neural Comput. Appl.*, vol. 34, no. 7, pp. 5649–5664, 2022, doi: 10.1007/s00521-021-06702-3.
- [16] S. Shao, W. Zhu, and Y. Li, "Radar Detection of Low-Slow-Small UAVs in Complex Environments," in *Proc. 2022 IEEE 10th Joint Int. Inf. Technol. Artif. Intell. Conf. (ITAIC)*, vol. 10, pp. 1153–1157, 2022, doi: 10.1109/ITAIC54216.2022.9836542.
- [17] S. Rudys *et al.*, "Hostile UAV Detection and Neutralization Using a UAV System," *Drones*, vol. 6, no. 9, 2022.
- [18] F. Svanström, F. Alonso-Fernandez, and C. Englund, "Drone detection and tracking in real-time by fusion of different sensing modalities," *Drones*, vol. 6, no. 11, p. 317, 2022, doi: 10.3390/drones6110317.
- [19] F. L. Chiper *et al.*, "Drone detection and defense systems: Survey and a software-defined radio-based solution," *Sensors*, vol. 22, no. 4, p. 1453, 2022, doi: 10.3390/s22041453.
- [20] C. Huang, I. Petrunin, and A. Tsourdos, "Radar-Camera Fusion for Ground-based Perception of Small UAV in Urban Air Mobility," in *Proc. 2023 IEEE 10th Int. Workshop Metrology AeroSpace (MetroAeroSpace)*, pp. 395–400, 2023.
- [21] C. Steffes, B. Demissie, M. Mandt, and M. Böswetter, "Surveillance of Critical Infrastructure using the LTE450 Network as Passive Radar Illuminator: Feasibility Study and Range Assessment," in *Proc. 2022 Sensor Data Fusion: Trends, Solut. Appl. (SDF)*, pp. 1–6, 2022, doi: 10.1109/SDF55338.2022.9931958.
- [22] Y. Lei, H. Yao, B. Jiang, T. Tian, and P. Xing, "Anti-UAV High-Performance Computing Early Warning Neural Network Based on PSO Algorithm," *Sci. Program.*, vol. 2022, 2022, doi: 10.1155/2022/7150128.
- [23] M. Rosamilia, A. Balleri, A. Maio, A. Aubry, and V. Carotenuto, "Radar Detection Performance Prediction Using Measured UAVs RCS Data," *IEEE Trans. Aerosp. Electron. Syst.*, vol. 59, pp. 3550–3565, 2023, doi: 10.1109/TAES.2022.3227224.
- [24] J. Zheng *et al.*, "An Efficient Strategy for Accurate Detection and Localization of UAV Swarms," *IEEE Internet Things J.*, vol. 8, pp. 15372–15381, 2021, doi: 10.1109/JIOT.2021.3064376.
- [25] P. Zhu *et al.*, "Detection and Tracking Meet Drones Challenge," in *IEEE Transactions on Pattern Analysis and Machine Intelligence*, vol. 44, no. 11, pp. 7380–7399, 1 Nov. 2022, doi: 10.1109/TPAMI.2021.3119563.
- [26] A. Aldowesh, T. Alnuaim, and A. Alzogaiby, "Slow-Moving Micro-UAV detection with a small scale Digital Array Radar," in *Proc. 2019 IEEE Radar Conf. (RadarConf)*, pp. 1–5, 2019, doi: 10.1109/RADAR.2019.8835567.
- [27] A. Coluccia, G. Parisi, and A. Fascista, "Detection and classification of multirotor drones in radar sensor networks: A review," *Sensors*, vol. 20, no. 15, p. 4172, 2020.
- [28] G. E. M. Abro, S. A. B. Zulkifli, R. J. Masood, V. S. Asirvadam, and A. Laouiti, "Comprehensive review of UAV detection, security, and communication advancements to prevent threats," *Drones*, vol. 6, no. 10, p. 284, 2022.
- [29] I. Iswanto and I. Ahmad, "Second order integral fuzzy logic control based rocket tracking control," *J. Robot. Control (JRC)*, vol. 2, no. 6, pp. 594–604, 2021.
- [30] A. Eldosouky, A. Ferdowsi, and W. Saad, "Drones in Distress: A Game-Theoretic Countermeasure for Protecting UAVs Against GPS Spoofing," *IEEE Internet Things J.*, vol. 7, pp. 2840–2854, 2019, doi: 10.1109/JIOT.2019.2963337.
- [31] K. Zhou, R. Wei, Q. Zhang, and Z. Wu, "Research on Decision-making Method for Territorial Defense Based on Fuzzy Reinforcement Learning," in *Proc. 2019 Chinese Autom. Congr. (CAC)*, pp. 3759–3763, 2019, doi: 10.1109/CAC48633.2019.8996813.
- [32] W. Khawaja, V. Semkin, N. I. Ratyal, Q. Yaqoob, J. Gul, and I. Guvenc, "Threats from and countermeasures for unmanned aerial and underwater vehicles," *Sensors*, vol. 22, no. 10, p. 3896, 2022.
- [33] J. Xie, Q. Fu, R. Jia, and M. Li, "Multi-UAV Path Planning under Radar Threats," in *Proc. 2023 IEEE Int. Conf. Smart Internet Things (SmartIoT)*, pp. 30–37, Aug. 2023.
- [34] V. P. Riabukha, "Radar surveillance of unmanned aerial vehicles," *Radioelectronics and Communications Systems*, vol. 63, no. 11, pp. 561–573, 2020.
- [35] D. Xing, Z. Zhen, and H. Gong, "Offense–defense confrontation decision making for dynamic UAV swarm versus UAV swarm," *Proc. Inst. Mech. Eng. G: J. Aerosp. Eng.*, vol. 233, pp. 5689–5702, 2019.
- [36] R. Aievola *et al.*, "Conflict Detection Performance of Ground-based Radar Networks for Urban Air Mobility," in *Proc. 2023 IEEE/AIAA 42nd Digit. Avion. Syst. Conf. (DASC)*, pp. 1–9, 2023, doi: 10.1109/DASC58513.2023.10311284.
- [37] Q. Xu, J. Ge, T. Yang, and X. Sun, "A trajectory design method for coupling aircraft radar cross-section characteristics," *Aerosp. Sci. Technol.*, vol. 98, p. 105653, 2020, doi: 10.1016/j.ast.2019.105653.
- [38] S. Singhal, S. Biswas, and S. Ram, "LEO/MEO-Based Multi-static Passive Radar Detection Performance Analysis Using Stochastic Geometry," in *Proc. 2023 IEEE Radar Conf. (RadarConf23)*, pp. 1–6, 2023, doi: 10.1109/RadarConf2351548.2023.10149574.
- [39] M. Kim *et al.*, "Toward Optimal Placement of Spatial Sensors to Detect Poisson-Distributed Targets," *IEEE Access*, vol. 11, pp. 121991–121998, 2023, doi: 10.1109/ACCESS.2023.3326349.
- [40] T. George, K. Wagner, and P. Rademacher, "Deep Q-network for radar task-scheduling problem," in *Proc. 2022 IEEE Radar Conf. (RadarConf22)*, pp. 1–5, March 2022.
- [41] J. Yan *et al.*, "Collaborative detection and power allocation framework for target tracking in multiple radar system," *Inf. Fusion*, vol. 55, pp. 173–183, 2020, doi: 10.1016/j.inffus.2019.08.010.
- [42] Y. Huang, Y. Shi, and T. Song, "An Efficient Multi-Path Multitarget Tracking Algorithm for Over-The-Horizon Radar," *Sensors (Basel)*, vol. 19, 2019, doi: 10.3390/s19061384.
- [43] X. Wang, B. Tang, and M. Zhang, "A Probabilistic Model-Based Robust Waveform Design for MIMO Radar Detection," in *Proc. 2021 CIE Int. Conf. Radar (Radar)*, pp. 1686–1690, 2021, doi: 10.1109/Radar53847.2021.10028035.
- [44] A. D. Brown, "Radar challenges, current solutions, and future advancements for the counter unmanned aerial systems mission," *IEEE Aerosp. Electron. Syst. Mag.*, vol. 38, no. 9, pp. 34–50, 2023.
- [45] H. Lan *et al.*, "Joint Target Detection and Tracking in Multipath Environment: A Variational Bayesian Approach," *IEEE Trans. Aerosp. Electron. Syst.*, vol. 56, pp. 2136–2156, 2019, doi: 10.1109/TAES.2019.2942706.
- [46] L. Gao, G. Battistelli, L. Chisci, and A. Farina, "Fusion-Based Multidetector Multitarget Tracking With Random Finite Sets," *IEEE Trans. Aerosp. Electron. Syst.*, vol. 57, pp. 2438–2458, 2021, doi: 10.1109/TAES.2021.3059093.
- [47] H. Zhang *et al.*, "Sensor Scheduling and Resource Allocation in Distributed MIMO Radar for Joint Target Tracking and Detection," *IEEE Access*, vol. 7, pp. 62387–62400, 2019, doi: 10.1109/ACCESS.2019.2916334.
- [48] J. Yan *et al.*, "Optimal Resource Allocation for Asynchronous Multiple Targets Tracking in Heterogeneous Radar Networks," *IEEE Trans. Signal Process.*, vol. 68, pp. 4055–4068, 2020, doi: 10.1109/TSP.2020.3007313.
- [49] J. Lee and J. Park, "Threat-Based Resource Allocation Strategy for Target Tracking in a Cognitive Radar Network," *arXiv preprint arXiv:2311.13906*, 2023, doi: 10.48550/arXiv.2311.13906.
- [50] G. Frazer and C. Williams, "Decametric Radar for Missile Defense," in *Proc. 2019 IEEE Radar Conf. (RadarConf)*, pp. 1–6, 2019, doi: 10.1109/RADAR.2019.8835810.
- [51] M. S. Ismail, A. Ahmad, S. Ismail, and N. M. M. Yusop, "A review on Unmanned Aerial Vehicle (UAV) threats assessments," in *AIP Conf. Proc.*, vol. 2617, no. 1, Nov. 2022.
- [52] L. Szarka and I. Harmati, "Swarm based drone umbrellas to counter missiles," in *Proc. 2020 23rd Int. Symp. Meas. Control Robot. (ISMCR)*, pp. 1–6, 2020, doi: 10.1109/ISMCR51255.2020.9263747.
- [53] G. Frazer and C. Williams, "Decametric Radar for Missile Defense," in *Proc. 2019 IEEE Radar Conf. (RadarConf)*, pp. 1–6, 2019, doi: 10.1109/RADAR.2019.8835810.
- [54] Y. Liu *et al.*, "Effective Capacity Based Power Allocation for the Coexistence of an Integrated Radar and Communication System and a Commercial Communication System," *IEEE Access*, vol. 8, pp. 58629–58644, 2020, doi: 10.1109/ACCESS.2020.2983328.

- [55] Z. Liu, Y. Lv, J. Zhou, and L. Hu, "On 3D simultaneous attack against manoeuvring target with communication delays," *Int. J. Adv. Robot. Syst.*, vol. 17, 2020, doi: 10.1177/1729881419894808.
- [56] D. Guo *et al.*, "Weapon-Target Assignment for Multi-to-Multi Interception With Grouping Constraint," *IEEE Access*, vol. 7, pp. 34838–34849, 2019, doi: 10.1109/ACCESS.2019.2898874.
- [57] V. Kurtz and H. Lin, "Toward Verifiable Real-Time Obstacle Motion Prediction for Dynamic Collision Avoidance," in *Proc. 2019 Am. Control Conf. (ACC)*, pp. 2633–2638, 2019, doi: 10.23919/ACC.2019.8815387.
- [58] I. S. Asti, T. Agustinah, and A. Santoso, "Obstacle avoidance with energy efficiency and distance deviation using KNN algorithm for quadcopter," in *Proc. 2020 Int. Seminar Intell. Technol. Its Appl. (ISITIA)*, pp. 285–291, July 2020.
- [59] D. Huo *et al.*, "Collision-Free Model Predictive Trajectory Tracking Control for UAVs in Obstacle Environment," *IEEE Trans. Aerosp. Electron. Syst.*, vol. 59, pp. 2920–2932, 2023, doi: 10.1109/TAES.2022.3221702.
- [60] Z. Niu, X. Jia, and W. Yao, "Communication-Free MPC-Based Neighbors Trajectory Prediction for Distributed Multi-UAV Motion Planning," *IEEE Access*, vol. 10, pp. 13481–13489, 2022, doi: 10.1109/ACCESS.2022.3148145.
- [61] X. Zhang *et al.*, "Trajectory Generation by Chance-Constrained Nonlinear MPC With Probabilistic Prediction," *IEEE Trans. Cybern.*, vol. 51, pp. 3616–3629, 2020, doi: 10.1109/TCYB.2020.3032711.
- [62] P. Wu, J. Xie, and J. Chen, "Safe Path Planning for Unmanned Aerial Vehicle under Location Uncertainty," in *Proc. 2020 IEEE 16th Int. Conf. Control Autom. (ICCA)*, pp. 342–347, 2020, doi: 10.1109/ICCA51439.2020.9264542.
- [63] B. Lindqvist, P. Sopasakis, and G. Nikolakopoulos, "A Scalable Distributed Collision Avoidance Scheme for Multi-agent UAV systems," in *Proc. 2021 IEEE/RSJ Int. Conf. Intell. Robots Syst. (IROS)*, pp. 9212–9218, 2021, doi: 10.1109/IROS51168.2021.9636293.
- [64] H. Huang *et al.*, "Cooperative Collision Avoidance Method for Multi-UAV Based on Kalman Filter and Model Predictive Control," in *Proc. 2019 IEEE Int. Conf. Unmanned Syst. Artif. Intell. (ICUSAI)*, pp. 1–7, 2019, doi: 10.1109/ICUSAI47366.2019.9124863.
- [65] J. Kim and Y. Kim, "Impact Time Control Guidance with Finite-Time Convergence Based on Pure Proportional Navigation," in *Proc. 2019 18th Eur. Control Conf. (ECC)*, pp. 143–148, 2019, doi: 10.23919/ECC.2019.8795943.
- [66] R. Wang and S. Tang, "Intercepting Higher-Speed Targets Using Generalized Relative Biased Proportional Navigation," *J. Northwest. Polytech. Univ.*, 2019, doi: 10.1051/jnwpu/20193740682.
- [67] N. Singh and S. Hota, "FOV constrained guidance law for nonstationary nonmaneuvering target interception with any impact angle," *Proc. Inst. Mech. Eng. G: J. Aerosp. Eng.*, vol. 236, pp. 1947–1960, 2021, doi: 10.1177/09544100211046867.
- [68] E. Kapeel *et al.*, "Evaluation of Missile Terminal Guidance Using Software in Loop (SIL)," in *Proc. 2020 12th Int. Conf. Electr. Eng. (ICEENG)*, pp. 389–395, 2020, doi: 10.1109/ICEENG45378.2020.9171703.
- [69] K. Song *et al.*, "A New Guidance Algorithm Against High-Speed Maneuvering Target," *Int. J. Aeronaut. Space Sci.*, pp. 1–13, 2021.
- [70] R. Zhang *et al.*, "IMMPDA Algorithm for Missile Tracking in Clutter," in *Proc. 2021 Int. Conf. Control Autom. Inf. Sci. (ICCAIS)*, pp. 178–182, 2021, doi: 10.1109/ICCAIS52680.2021.9624617.
- [71] Y. Wang, H. Wang, D. Lin, and W. Wang, "Nonlinear modified bias proportional navigation guidance law against maneuvering targets," *Journal of the Franklin Institute*, vol. 359, no. 7, pp. 2949–2975, 2022.
- [72] H. Shin and K. Li, "An Improvement in Three-Dimensional Pure Proportional Navigation Guidance," *IEEE Trans. Aerosp. Electron. Syst.*, vol. 57, pp. 3004–3014, 2021, doi: 10.1109/TAES.2021.3067656.
- [73] N. K. Singh and S. Hota, "Time-optimal moving target interception with impact angle constraint," *Proceedings of the Institution of Mechanical Engineers, Part G: Journal of Aerospace Engineering*, vol. 237, no. 7, pp. 1600–1613, 2023.
- [74] A. Ranjan, S. Hota, and N. Singh, "Three-Stage Proportional Navigation for Intercepting Stationary Targets with Impact Angle Constraints," in *Proc. 2019 Sixth Indian Control Conf. (ICC)*, pp. 379–384, 2019, doi: 10.1109/ICC47138.2019.9123163.
- [75] V. Markevich and V. Legkostup, "Modified method of proportional navigation to intercept aeroballistic targets with a limited sector guidance of missile," *Syst. Anal. Appl. Inf. Sci.*, vol. 4, pp. 28–50, 2019.
- [76] J. Wu, W. Yuan, and L. Bai, "On the Interplay Between Sensing and Communications for UAV Trajectory Design," *IEEE Internet Things J.*, vol. 10, pp. 20383–20395, 2023, doi: 10.1109/JIOT.2023.3287991.
- [77] H. Yang *et al.*, "A Distributed Cooperative Tracking Algorithm for the Interception of Small Patrol UAVs," in *Proc. 2023 42nd Chinese Control Conf. (CCC)*, pp. 3859–3865, 2023.
- [78] L. Ding *et al.*, "Research on Collaborative Detection and Location Method of Infrared and Radar Aircraft Based on Federated Filter," in *Proc. 2021 6th Int. Conf. Multimedia Syst. Signal Process.*, 2021, doi: 10.1145/3471261.3471271.
- [79] C. Yu *et al.*, "Research on Strategy of Breaking Through Multi-UAV Defense," in *Proc. 2021 33rd Chinese Control Decis. Conf. (CCDC)*, pp. 7525–7531, 2021, doi: 10.1109/CCDC52312.2021.9601995.
- [80] Y. Luo *et al.*, "UAV-Cooperative Penetration Dynamic-Tracking Interceptor Method Based on DDPG," *Appl. Sci.*, vol. 12, no. 3, p. 1618, 2022, doi: 10.3390/app12031618.
- [81] M. Kratky *et al.*, "Electronic Warfare Methods Combatting UAVs," *Adv. Sci. Technol. Eng. Syst. J.*, vol. 5, pp. 447–454, 2020.
- [82] J. Goricaneč *et al.*, "Collision-Free Trajectory Following With Augmented Artificial Potential Field Using UAVs," *IEEE Access*, vol. 11, pp. 83492–83506, 2023, doi: 10.1109/ACCESS.2023.3303109.
- [83] H. Xie *et al.*, "Three-Dimensional Path Planning of UAV Based on Improved Artificial Potential Field," in *Proc. 2021 40th Chinese Control Conf. (CCC)*, pp. 7862–7867, 2021.
- [84] C. Kownacki, "Artificial Potential Field Based Trajectory Tracking for Quadcopter UAV Moving Targets," *Sensors*, vol. 24, no. 4, p. 1343, 2024.
- [85] X. Lu, "Improved path planning method for unmanned aerial vehicles based on artificial potential field," *Appl. Comput. Eng.*, vol. 10, no. 1, pp. 64–71, 2023, doi: 10.54254/2755-2721/10/20230142.
- [86] X. Fang *et al.*, "JTEA: A Joint Trajectory Tracking and Estimation Approach for Low-Observable Micro-UAV Monitoring With 4-D Radar," *IEEE Trans. Instrum. Meas.*, vol. 73, pp. 1–14, 2024, doi: 10.1109/TIM.2023.3338650.
- [87] Z. Xia *et al.*, "Multi-Agent Reinforcement Learning Aided Intelligent UAV Swarm for Target Tracking," *IEEE Trans. Veh. Technol.*, vol. 71, pp. 931–945, 2022, doi: 10.1109/TVT.2021.3129504.
- [88] J. Zhang *et al.*, "A Many-to-Many UAV Pursuit and Interception Strategy Based on PERMADDPG," in *Proc. 2023 5th Int. Conf. Robot. Comput. Vis. (ICRCV)*, pp. 234–240, 2023, doi: 10.1109/ICRCV59470.2023.10329206.
- [89] X. Wang *et al.*, "An Optimal Guidance Strategy for Moving-Target Interception by a Multirotor Unmanned Aerial Vehicle Swarm," *IEEE Access*, vol. 8, pp. 121650–121664, 2020, doi: 10.1109/ACCESS.2020.3006479.
- [90] M. Sahal, V. C. Maynad, and Y. Bilfaqih, "Cooperative Formation and Obstacle Avoidance Control for Multi-UAV Based on Guidance Route and Artificial Potential Field," *J. Robot. Control (JRC)*, vol. 5, no. 6, pp. 1772–1783, 2024.
- [91] S. Nurjanah, T. Agustinah, and M. Fuad, "Cooperative position-based formation-pursuit of moving targets by multi-UAVs with collision avoidance," *JAREE (J. Adv. Res. Electr. Eng.)*, vol. 6, no. 2, 2022.
- [92] M. Sahal, T. Agustinah, and A. Jazidie, "Switching formation and topology in cooperative multi-agent source seeking using gradient estimation," in *Proc. 2019 Int. Conf. Artif. Intell. Inf. Technol. (ICAIIIT)*, pp. 151–156, 2019, doi: 10.1109/ICAIIIT.2019.9123163.
- [93] C. Xu, M. Xu, and C. Yin, "Optimized multi-UAV cooperative path planning under the complex confrontation environment," *Comput. Commun.*, vol. 162, pp. 196–203, 2020.
- [94] Z. Tian *et al.*, "Missile Threat Detection and Evasion Maneuvers With Countermeasures for a Low-Altitude Aircraft," *IEEE Trans. Aerosp. Electron. Syst.*, vol. 59, no. 6, pp. 7352–7362, 2023.